Applied Physics Letters

Strong enhancement of room-temperature thermoelectric properties of Cu-doped $Bi_2Te_{2.7}Se_{0.3}$

Cite as: Appl. Phys. Lett. **120**, 043903 (2022); https://doi.org/10.1063/5.0077057
Submitted: 29 October 2021 • Accepted: 13 January 2022 • Published Online: 25 January 2022

Gwansik Kim, Kyungmi Lee, Hyunjun Shin, et al.

Applied Physics Letters ARTICLE scitation.org/journal/apl

Strong enhancement of room-temperature thermoelectric properties of Cu-doped $Bi_2Te_{2.7}Se_{0.3}$

Cite as: Appl. Phys. Lett. **120**, 043903 (2022); doi: 10.1063/5.0077057
Submitted: 29 October 2021 · Accepted: 13 January 2022 ·
Published Online: 25 January 2022

Gwansik Kim,[1,2] Kyungmi Lee,[1] Hyunjun Shin,[1] Jeongmin Kim,[3] Joonyeon Chang,[1,4] Jong Wook Roh,[5,a)] and Wooyoung Lee[1,6,a)]

AFFILIATIONS

[1]Department of Materials Science and Engineering, Yonsei University, Seoul 03722, Republic of Korea
[2]Advanced Materials Research Team, Hyundai Motor Company, 37 Cheoldobangmulgwan-ro, Uiwang-si, Gyeonggi-do 16082, Republic of Korea
[3]DGIST, 333 Techno Jungang-daero, Hyeonpung-eup, Dalseong-gun, Daegu 42988, Republic of Korea
[4]Natural Products Institute, Korea Institute of Science and Technology (KIST), 679 Saimdang-ro, Gangneung, Gangwon-do 25451, Republic of Korea
[5]School of Nano and Materials Science and Engineering, Kyungpook National University, Gyeongsangbuk-do 37224, Republic of Korea
[6]Center for Spintronics, Post-silicon Semiconductor Insitute, Korea Institute of Science and Technology, Seoul 02792, Republic of Korea

[a)]**Authors to whom any correspondence should be addressed:** jw.roh@knu.ac.kr and wooyoung@yonsei.ac.kr

ABSTRACT

We investigate thermoelectric properties of Cu-doped $Bi_2Te_{2.7}Se_{0.3}$ fabricated using a simple doping process and spark plasma sintering. Through precise control of Cu doping, it is found that Cu atoms preferentially occupied Bi sites and then intercalated into the van der Waals gap with an increasing Cu content. Electrical transport properties of Cu-doped samples were systemically controlled using this mechanism. At the same time, thermal conductivities of the Cu-doped samples were reduced by the enhancement of point defect phonon scattering due to the Cu atoms. Compared to that of pristine samples, the dimensionless thermoelectric figure of merit ("*ZT*") of 0.98 at 323 K for the Cu-doped sample was increased by more than 92% owing to these synergetic effects. Furthermore, the shift of maximum *ZT* to room temperature provides advantages for enlarging the applications of thermoelectric effects at room temperature.

Thermoelectric (TE) materials have been the focus of recent research owing to their potential for energy harvesting and solid-state refrigeration.[1,2] The energy conversion efficiency of TE materials can be evaluated as the dimensionless figure of merit $ZT = \sigma S^2 T/\kappa_{tot}$, where σ, S, κ_{tot}, and T represent the electrical conductivity, Seebeck coefficient, total thermal conductivity, and absolute temperature, respectively. Continuous efforts have been made to enhance *ZT* in Bi_2Te_3-based materials, which are the most well-known TE materials in the low-temperature range (<450 K).[3–6] In *p*-type materials (ternary alloy $Bi_{0.5}Sb_{1.5}Te_3$), high *ZT* values of 1.2–1.6 have been achieved using phonon engineering[7–10] and band engineering[11–13] by introduction of nanoscale microstructures. However, in the case of *n*-type TE materials such as $Bi_2Te_{2.7}Se_{0.3}$ (BTS), introducing microstructures was less effective for enhancing the *ZT* values and reproducibility because of the uncontrollable defect generation. Liu *et al.* found that the intercalation of Cu could significantly improve the reproducibility of BTS by suppressing the escape of Te atoms.[14] Although Cu-intercalation in *n*-type TE materials is an effective method for enhancing the reproducibility, the *ZT* values of *n*-type TE materials are still low compared to those of *p*-type TE materials. Lee *et al.* obtained a *ZT* of 0.91 at 320 K for $Cu_{0.008}Bi_{1.99}Au_{0.01}Te_{2.7}Se_{0.3}$ through significant improvement of the Seebeck coefficient by Au doping on the Bi site, suggesting the possibility of enhancing *ZT*.[15] In this report, Lee *et al.* also reported that the enhancement of the TE properties in polycrystalline *n*-type BTS can be enhanced by the intercalation of Cu and the doping of Al on Bi-sites. Despite this careful study, the mechanism of *ZT* enhancement in Cu-doped BTS is still not clear.

Herein, we systematically study the effect of Cu doping on the electrical and thermal properties of Cu-doped BTS. The *ZT* values were significantly enhanced over a wide temperature range through Cu doping by the simultaneous manipulation of the electronic and thermal transport properties. The peak value of *ZT* was measured to

be 0.98 at 323 K for the 0.2 vol. % Cu-doped BTS sample. Moreover, the peak of *ZT* shifted from a higher temperature to room temperature mainly because of the modification of thermal conductivities for the Cu-BTS samples. This shift of the maximum *ZT* makes it feasible to expand the applications of TE materials and devices at room temperature.

Cu-doped BTS samples (Cu 0.025–0.5 vol. %) were fabricated by metal acetate doping[16–18] and spark plasma sintering (SPS). To analyze the Cu doping effect of *n*-type BTS alloys and minimize the range of deviations in TE properties, we purchased commercial BTS-based ingots made by the zone melting process (LIVINGCARE Co., Ltd.). The BTS-based ingots were crushed into powders using a ball mill (Pulverisette 7, Fritsch GmbH, Germany) for 10 min under an argon atmosphere, and then the size of the milled powders was controlled by sieving (<53 μm). For the doping of Cu atoms into the BTS powders, copper (II) acetate [$(CH_3COO)_2Cu$, Alfa Aesar] was used as the dopant material. A high-energy ball milling process (8000D, SPEX, USA) was carried out for 5 min in an argon atmosphere to homogeneously deposit copper (II) acetate onto the surface of the BTS powder. Then, to reduce the acetate (–CH_3COO–), heat treatment was conducted in a tube-type furnace under a mixed gas atmosphere (95% N_2 and 5% H_2) at 573 K for 3 h. The polycrystalline compacted Cu-doped BTS bulks were prepared by SPS under 30 MPa pressure at 773 K for 2 min in vacuum.

Phase analysis of the Cu-doped BTS samples was carried out using x-ray diffraction (XRD) (Ultima IV/ME 200DX, Rigaku, Japan) with CuKα radiation. Raman spectroscopy was employed to clarify the Cu doping sites using a 532 nm Nd:YAG laser (LabRam Aramis, Horriba Jovin Yvon, France). A field emission scanning electron microscope (FE-SEM, JEOL-7001F, JEOL, Ltd., Japan) was used to observe the microstructure of the fractured bulk surface. Low-magnification TEM, selected area electron diffraction (SAED) pattern analysis, and scanning transmission electron microscopy (STEM)-high-angle annular dark field (HAADF) analysis (STEM; JEM-ARM 200F, JEOL, Ltd., Japan) were performed to clarify the atomic sites of Cu dopants and various defects. Hall effect measurements were conducted in the van der Pauw configuration under a constant magnetic field (1 T) at 303 K. The Hall mobility (μ_{Hall}) and concentration (n_c) were calculated using the one-band model without considering minority carriers. The temperature dependences of σ and S of the Cu-doped BTS samples were measured using a TE property measurement system (ZEM-3, ULVAC, Japan) between 303 and 483 K. The κ_{tot} values were calculated using the equation $\kappa_{tot} = \rho_s C_p \lambda$, where ρ_s is the density, C_p is the specific heat capacity, and λ is the thermal diffusivity. λ was measured in a vacuum using the laser flash method (LFA-457, Netzsch, Germany), and C_p was assigned a constant value of 0.157 J g^{-1} K^{-1}.

Figure 1(a) shows the x-ray diffraction patterns of Cu-doped BTS samples (Cu 0.025–0.5 vol. %). All patterns were indexed with a targeted rhombohedral $R\bar{3}m$ space group as the major phase. Secondary phases were not detected in any of the samples, indicating that Cu was

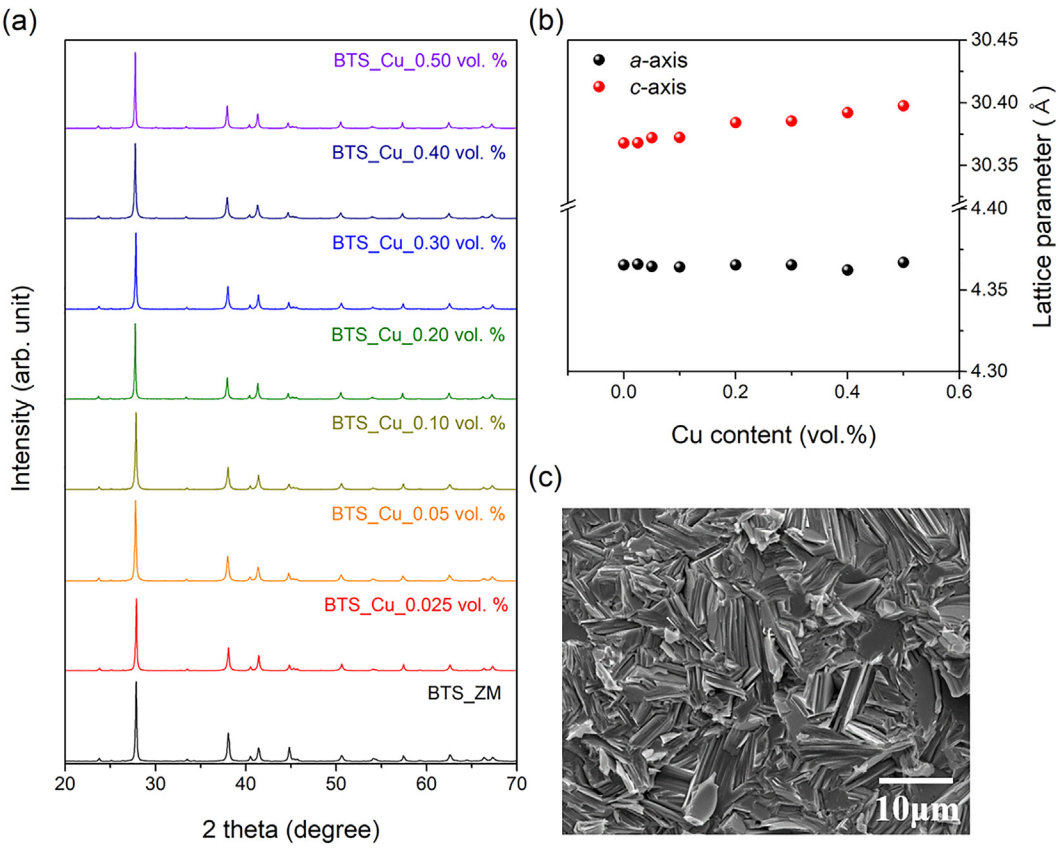

FIG. 1. (a) Powder XRD patterns and (b) the variation in lattice parameters of the Cu-doped BTS samples. (c) SEM image of the fractured surface of the 0.3 vol. % Cu-doped BTS sample.

readily soluble in the BTS lattice. It should be noted that the *c*-axis lattice parameter for Cu-doped BTS samples tends to slightly increase with increasing Cu content, as shown in Fig. 1(b). The change in the *c*-axis lattice parameter was not noticeable in samples with a Cu content under 0.2 vol. %, but the change was significant in the samples with higher Cu contents. This increase in the *c*-axis lattice parameter in the samples with higher Cu contents is attributed to the intercalation of Cu atoms into the van der Waals (vdW) gap. This result is in agreement with a previous report that Cu atoms preferentially occupy Bi sites and then intercalate into the vdW gap with the increasing Cu content.[19] To clarify this, we measured the Raman spectra of the Cu-doped BTS samples. As shown in Fig. S1, three vibration modes at 62.2 cm^{-1} (A_{1g}^1), 103.12 cm^{-1} (E_g^2), and 135.32 (A_{1g}^2) were found in all Cu-doped BTS samples.[20] However, the A_{1g}^1 and A_{1g}^2 modes gradually decrease with the increase in the Cu content. This indicates that the preferential occupation of Cu dopants changes from substitution for the Bi sites to intercalation in vdW gaps with the increasing Cu content, because the out-of-plane vibration was suppressed by the Cu intercalations. The SEM images of the fractured surface of the Cu-doped BTS samples demonstrate polycrystalline structures with clean and fine-layered microstructures [Fig. 1(c)]. As shown in Fig. S2, all the Cu-doped BTS samples have similar microstructures at the micro-scale level. We prepared an ultra-thin TEM sample of the 0.4 vol. % Cu-doped BTS sample using a precision ion polishing system (PIPS 691, Gatan, USA) to observe the large-area atomic scale microstructure (Fig. S3 in the supplementary material). The atomic arrangement of Bi_2Te_3 and the vdW gap between the $Te^{(1)}$: $Te^{(1)}$ planes was observed.[21–23] Unfortunately, because of the difficulties in the sample preparation process, we could not distinguish the various atomic defects such as interstitials, anti-site defects, and vacancies.

An in-depth analysis of the electronic and thermal transport properties should be carried out to investigate the doping effect and doping mechanism of Cu in a BTS alloy. In this study, we fabricated three different samples of each composition to evaluate their TE properties. The electronic transport properties [σ, S, and power factor (PF)] as a function of temperature for the Cu-doped BTS samples are shown in Fig. 2. The σ values of the Cu-doped BTS samples were lower than those of the pristine sample. At 303 K, it should be noted that σ decreases with the increasing Cu content up to 0.3 vol. % and then begins to increase again for Cu doping levels greater than 0.3 vol. % [Fig. 3(a)]. To clarify this, the Hall effect parameters of the Cu-doped BTS samples were investigated to calculate the carrier concentrations (n_c) and Hall mobilities (μ_{Hall}) by estimating the one-band model without considering minor carriers, as presented in Table S1. The n_c values of the Cu-doped BTS samples continuously decreased until the Cu content reached 0.3 vol. % (6.18×10^{19}–1.62×10^{19} cm^{-3}). After that, the n_c values in the Cu-doped BTS samples with Cu content over 0.3 vol. % recovered slightly from 1.62×10^{19} cm^{-3} to 3.01×10^{19} cm^{-3}. At the same time, the μ_{Hall} values generally increased from 166.46 to 257.11 cm^2 V^{-1} s^{-1} with the increase in the Cu content. From these results, we can infer that the Cu doping mechanism was changed in the samples with the increasing Cu doping content. It seems that Cu atoms preferentially occupy Bi sites in the case of doping at lower Cu levels (0.025–0.3 vol. %). The occupation of Cu atoms at Bi sites leads to the reduction of n_c, generating one hole per Cu atom.[19] On the other hand, it seems that Cu intercalation defects compensate for the hole carriers induced by the occupation of Cu atoms at Bi sites, resulting in the recovery of n_c, as shown in Fig. 3(b). This Cu intercalation is in good agreement with the results of the XRD investigation [Fig. 1(b)], which shows that the lattice parameter of the *c*-axis was slightly enlarged in the samples with high levels of Cu doping. Under these conditions, the lattice parameter of the *a*-axis was independent of the Cu content. The μ_{Hall} values of the Cu-doped BTS samples increased steadily with the increasing Cu content by 0.4 vol. %, showing a different tendency from that of n_c, as shown in Fig. 3(b) and Table S1. In general, the intercalated Cu atoms in the vdW gap of the BTS alloys result in the enhancement of μ_{Hall} owing to the conductive two-dimensional channels.[24] However, the μ_{Hall} behavior in the 0.5 vol. % Cu-doped BTS sample may be slightly different because of a Cu-based secondary phase or some other doping mechanisms.

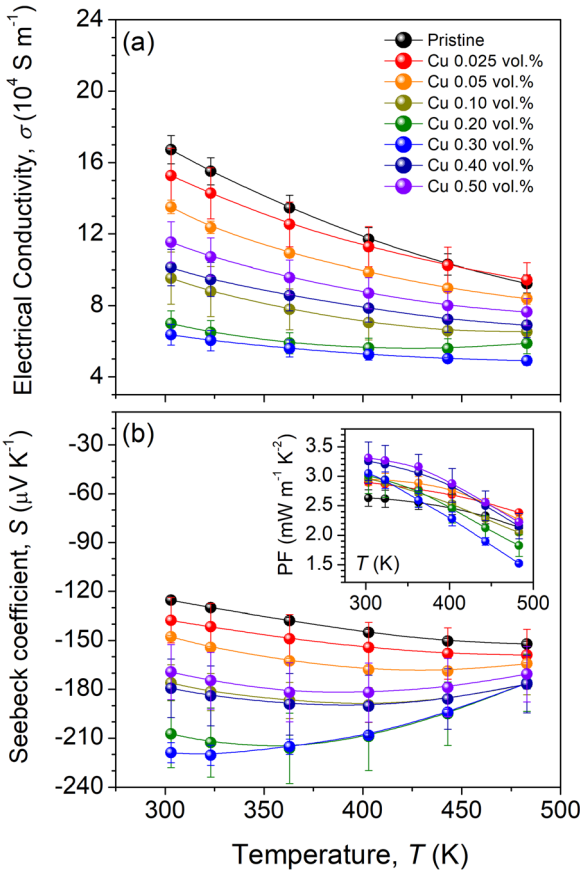

FIG. 2. Temperature dependences of the (a) electrical conductivity and (b) Seebeck coefficient of the Cu-doped BTS samples. The inset in (b) shows the temperature dependence of the power factor.

The *n*-type semiconductor properties of the Cu-doped BTS samples were confirmed by investigating the Seebeck coefficient, as shown in Fig. 2(b). The S values of the Cu-doped BTS samples were negative and higher than those of the pristine sample. In contrast to σ, the absolute S values increased up to 0.3 vol. % of the Cu content and then decreased in the samples with higher Cu contents [Fig. 3(a)]. This opposite tendency originates from the trade-off relationship between S and n_c according to the following equation:

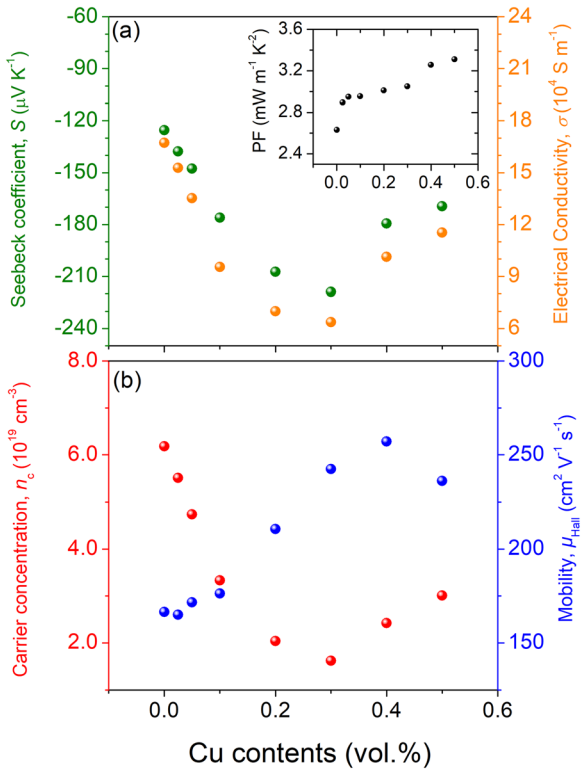

FIG. 3. Cu content dependences of the (a) electrical conductivity and Seebeck coefficient and (b) carrier concentration and Hall mobility of the Cu-doped BTS samples. The inset in (a) shows the Cu content dependence of the power factor.

$$S = \frac{8\pi^2 k_B^2}{3eh^2}\left(\frac{\pi}{3n_c}\right)^{2/3} m^* T,$$

where k_B, e, and h are the Boltzmann constant, elementary charge, and the Planck constant, respectively. The temperature dependence of the *PF* was calculated from the measured σ and S values as shown in the inset of Fig. 2(b). As the Cu content increased, the *PF* at 303 K gradually increased [the inset of Fig. 3(a)] owing to the optimized σ and S. By manipulating n_c with Cu contents, we could obtain the maximized *PF* values.

To achieve a high *ZT* value, the thermal transport properties should be considered along with the electrical properties such as σ and S. The effect of Cu doping on the thermal conductivities of BTS alloys was investigated using the laser flash method. Figure 4(a) shows the temperature dependence of κ_{tot} for the Cu-doped BTS samples. In Fig. 4(a), κ_{tot} values of the Cu-doped BTS samples were lower (1.34 W m^{-1} K^{-1} for 0.025 vol. %, 0.96 W m^{-1} K^{-1} for 0.2 vol. % at 303 K) than that of the pristine sample (1.71 W m^{-1} K^{-1} at 303 K) over the entire range of the measured temperature. Moreover, the minimum peak of κ_{tot} shifts to room temperature from higher temperatures, mainly because of the increase in the bipolar thermal conduction by the decreased concentration of the majority carriers (electrons). We calculated $\kappa_{lat}+\kappa_{bp}$ values to clarify the phonon scattering effect. The κ_{ele} value was obtained using the Wiedemann–Franz law ($\kappa_{ele} = L\sigma T$, where L is the Lorenz number). L was estimated using the following equation:[25]

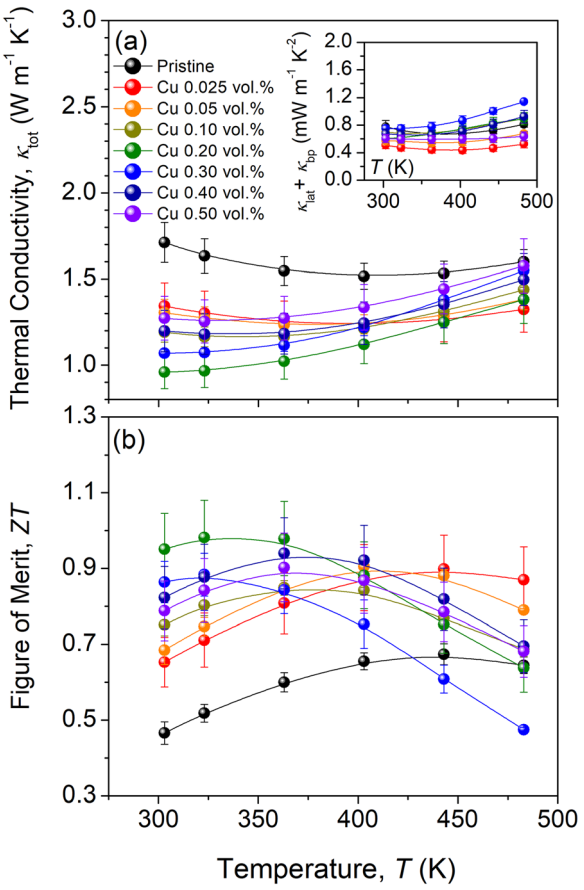

FIG. 4. Temperature dependences of the (a) thermal conductivity and (b) dimensionless figure of merit *ZT* of the Cu-doped BTS samples. The inset in (a) shows the temperature dependence of $\kappa_{lat}+\kappa_{bp}$.

$$L = 1.5 + \exp\left[-\frac{|S|}{116}\right],$$

where L and S are 10^{-8} W Ω K^{-2} and μV K^{-1}, respectively. The temperature dependence of $\kappa_{lat}+\kappa_{bp}$ for the Cu-doped BTS samples is shown in the inset of Fig. 4(a). Most values of $\kappa_{lat}+\kappa_{bp}$ for the Cu-doped BTS samples were lower than that of the pristine sample because of the intensified point-defect phonon scattering. However, the high $\kappa_{lat}+\kappa_{bp}$ values of the Cu-doped BTS samples with low n_c were attributed to bipolar thermal conduction. The dimensionless figures of merit *ZT* of the Cu-doped BTS samples are shown in Fig. 4(b). The *ZT* values were significantly enhanced over a wide temperature range by doping with Cu. The maximum *ZT* was 0.98 at 323 K for the 0.2 vol. % Cu-doped BTS sample. Considering that the *ZT* at 323 K for the pristine sample was approximately 0.5, the maximum *ZT* increased by more than 92%. This *ZT* enhancement of the Cu-doped BTS samples was caused by the simultaneous manipulation of the electronic and thermal transport properties. Notably, a shift in the maximum *ZT* was observed at room temperature in the Cu-doped BTS samples, mainly due to the thermal transport properties.

In conclusion, the electrical and thermal properties of Cu-doped BTS fabricated by the simple doping process were investigated, and the *ZT* values were significantly enhanced by the Cu-doping. This enhancement of *ZT* was mainly caused by the combined effect of the increase in the *PF* and the reduction in the thermal conductivity. The maximum *ZT* was 0.98 at 323 K owing to these synergetic effects. It should be noted that the maximum *ZT* value increased by more than 92% at 323 K. The shift of the maximum *ZT* to room temperature in the Cu-doped BTS samples sheds some light on the transport mechanism in this prospective high-efficiency TE material.

See the supplementary material for information on the Cu-doped BTS sample structure analyzed using Raman spectroscopy, SEM images, TEM image, SAED pattern, and STEM-HAADF image.

This work was supported by the Yonsei-KIST Institutional Program (Project No. 2Z06430-20-P069); the Technology Innovation Program (No. "20013621," Center for Super Critical Material Industrial Technology) funded by the Ministry of Trade, Industry, and Energy (MOTIE, Korea); and the National Research Foundation of Korea (NRF) grant funded by the Korea government (MSIT) (Nos. NRF-2018R1D1A1A02085389, NRF-2019R1A6A1A11055660, and NRF-2021R1A5A8033165).

AUTHOR DECLARATIONS

Conflict of Interest

The authors have no conflicts to disclose.

Author Contributions

G.K. and K.L. contributed equally to this work.

DATA AVAILABILITY

The data that support the findings of this study are available within the article and its supplementary material.

REFERENCES

[1]L. E. Bell, Science **321**(5895), 1457 (2008).
[2]J. He and T. M. Tritt, Science **357**(6358), eaak9997 (2017).
[3]B. Poudel, Q. Hao, Y. Ma, Y. C. Lan, A. Minnich, B. Yu, X. A. Yan, D. Z. Wang, A. Muto, D. Vashaee, X. Y. Chen, J. M. Liu, M. S. Dresselhaus, G. Chen, and Z. F. Ren, Science **320**(5876), 634 (2008).
[4]G. J. Snyder and E. S. Toberer, Nat Mater **7**(2), 105 (2008).
[5]M. Martín-González, O. Caballero-Calero, and P. Díaz-Chao, Renewable Sustainable Energy Rev. **24**, 288 (2013).
[6]T. M. Tritt, Science **283**(5403), 804 (1999).
[7]S. I. Kim, K. H. Lee, H. A. Mun, H. S. Kim, S. W. Hwang, J. W. Roh, D. J. Yang, W. H. Shin, X. S. Li, Y. H. Lee, G. J. Snyder, and S. W. Kim, Science **348**(6230), 109 (2015).
[8]Y. Li, X. Wang, G. Liu, B. Shin, and F. Shan, Scr. Mater. **172**, 88 (2019).
[9]C. Tan, X. Tan, F. Shi, Y. Yin, G.-Q. Liu, C. Xiong, H. Wang, G. Luo, B. Yu, J. G. Noudem, B. Liang, and J. Jiang, Ceram. Int. **47**(1), 725 (2021).
[10]X. F. Tang, W. J. Xie, H. Li, W. Y. Zhao, Q. J. Zhang, and M. Niino, Appl. Phys. Lett. **90**(1), 012102 (2007).
[11]L.-P. Hu, T.-J. Zhu, Y.-G. Wang, H.-H. Xie, Z.-J. Xu, and X.-B. Zhao, NPG Asia Mater. **6**(2), e88 (2014).
[12]K. Kim, G. Kim, H. Lee, K. H. Lee, and W. Lee, Scr. Mater. **145**, 41 (2018).
[13]W. H. Shin, J. W. Roh, B. Ryu, H. J. Chang, H. S. Kim, S. Lee, W. S. Seo, and K. Ahn, ACS Appl. Mater. Interface **10**(4), 3689 (2018).
[14]W. S. Liu, Q. Y. Zhang, Y. C. Lan, S. Chen, X. Yan, Q. Zhang, H. Wang, D. Z. Wang, G. Chen, and Z. F. Ren, Adv. Energy Mater. **1**(4), 577 (2011).
[15]K. H. Lee, S. I. Kim, H. Mun, B. Ryu, S. M. Choi, H. J. Park, S. Hwang, and S. W. Kim, J. Mater. Chem. C **3**(40), 10604 (2015).
[16]G. Kim, H.-S. Kim, H. S. Lee, J. Kim, K. H. Lee, J. W. Roh, and W. Lee, Nano Energy **72**, 104698 (2020).
[17]G. Kim, H. Lee, H. J. Rim, J. Kim, K. Kim, J. W. Roh, S. M. Choi, B. W. Kim, K. H. Lee, and W. Lee, J. Alloy Compd. **769**, 53 (2018).
[18]Y. Lin, K. A. Watson, M. J. Fallbach, S. Ghose, J. G. Smith, D. M. Delozier, W. Cao, R. E. Crooks, and J. W. Connell, ACS Nano **3**(4), 871 (2009).
[19]Y. M. Kim, K. H. Lee, L. Fu, M. W. Oh, S. H. Yang, S. Ning, G. Han, M. Y. Kim, J. S. Kim, M. Jeong, J. Jang, E. Lee, E. Okunishi, H. Sawada, S. i Kim, S. J. Pennycook, Y. H. Lee, and S. W. Kim, Mater. Today Phys. **17**, 100347 (2021).
[20]F. J. Liu, L. Y. Hu, M. Karakaya, P. Puneet, R. Rao, R. Podila, S. Bhattacharya, and A. M. Rao, Sci. Rep. **7**, 16535 (2017).
[21]A. S. Epstein, H. Fritzsche, and K. Lark-Horovitz, Phys. Rev. **107**(2), 412 (1957).
[22]D. Haneman, Phys. Rev. **119**(2), 567 (1960).
[23]R. M. Martin, G. Lucovsky, and K. Helliwell, Phys. Rev. B **13**(4), 1383 (1976).
[24]F. K. Aleskerov, K. S. Kakhramanov, and S. S. Kakhramanov, Inorg. Mater. **48**(5), 456 (2012).
[25]H. S. Kim, Z. M. Gibbs, Y. L. Tang, H. Wang, and G. J. Snyder, APL Mater. **3**(4), 041506 (2015).